IN-71-CR

239254

Acoustical Effects of a Large Ridge on Low-frequency Sound Propagation in Stationary and Moving Atmospheres

298

by

J. S. Robertson, M. J. Jacobson,
W. L. Siegmann and D. P. Santandrea

NAG1-929

Department of Mathematical Sciences

Rensselaer Polytechnic Institute

Troy, NY 12180-3590

RPI Math. Rep. No. 181

November 20, 1989

This work is sponsored by

National Aeronautics and Space Administration

Langley Research Center

Research Grant No. NAG-1-929

ABSTRACT

The effects of a ridge on a low-frequency acoustic propagation in quiescent and windy atmospheres are investigated using a parabolic approximation. A logarithmic wind-speed profile, commonly employed to model atmospheric wind currents, is modified and used to model two-dimensional atmospheric flow over a triangularly-shaped hill. The parabolic equation is solved using an implicit finite-difference algorithm. Several examples are examined to determine the combined effects of source-ridge distance, ridge dimensions, wind-speed profile, and cw source frequency on the received acoustic field.

INTRODUCTION

Low-frequency sound propagation in the atmosphere has many important applications. For example, wind turbines, such as those at the NASA facility at Medicine Bow, Wyoming, can act as strong sources of low frequency acoustic signals. These wind turbines consist of two forty-meter blades attached to a generator which is mounted atop a support tower eighty meters high. As the blades rotate, impulsive aerodynamic loads change along the blade as it passes through the turbulent wake of the support tower. It has been shown that the blade tip functions as a point source of low-frequency noise as it passes through the wake, forty meters above the ground. The frequency range for this source is between 1 Hz and 20 Hz.[1] Furthermore, low-frequency propagation can be important in military applications in which passive acoustic sensors exploit portions of the generated acoustic spectra to detect, locate, and track rotary-wing aircraft and ground vehicles.[2,3] Low-frequency signals from such sources can also propagate to long distances and interact with buildings and other structures to generate substantial amounts of undesirable secondary noise.[4]

While ray theory has seen extensive use in atmospheric acoustics, other models, such as the parabolic approximation and the fast-field program are more appropriate for use at frequencies where diffraction effects may be important. Of these two approaches, the parabolic approximation, which has been broadly applied to numerous ocean-acoustics problems, is well-suited for handling range-dependent propagation environments. This model has been used to examine atmospheric propagation by us and others in several recent studies. [5-9]

The purpose of this paper is to examine two-dimensional low-frequency sound propagation over hills in both quiescent and moving atmospheres. Because the topography of the earth-air interface is range-dependent, and because diffraction of the sound field behind the ridge can be important, we elect to use the parabolic approximation as the acoustic model for this study. Previous theoretical and experimental studies have examined the problem of sound over screens and wedge-shaped barriers. However, the focus of this work was typically at frequencies an order of magnitude or more higher and at ranges an order of magnitude or

more smaller than those with which we are concerned in this paper. In ocean acoustics, the somewhat analogous problem of propagation over a seamount has been considered.[10] In the deep ocean however, sound propagates over seamounts in an entirely different way as a result of the presence of the SOFAR channel.[11,12] In contrast, atmospheric sound can interact strongly with the ground surface, particularly in the presence of a wind. Some earlier theoretical studies used the geometrical theory of diffraction to examine sound propagation over a ground barrier which was modeled as a triangular wedge. However, the results were not valid near or on the wedge face away from the source, or on the ground surface close to the trailing barrier edge.[13,14] A description of the sound field in these regions is desirable, and this can be provided with reasonable accuracy by the parabolic approximation.

In Sec. I, we review briefly the parabolic approximation and formulate both the idealized ridge topography and wind profile. Then, in Sec. II, we examine the results of propagation predictions for a variety of source locations and environmental situations. The relative intensity is computed in quiescent environments, as well as windy ones in which the wind blows both toward and away from the receiver. Finally, we then summarize the principal results of our paper.

1. ACOUSTIC, GROUND, AND WIND MODELS

Let $p(r,z)$ be the acoustic pressure caused by the presence of a cw point source S in a moving atmosphere, where r and z denote range and height in cylindrical coordinates. We will confine our attention to a vertical plane containing the source and the wind velocity. As shown in Fig. 1, the origin of the r-z coordinate system is on the ground below the source. The ground surface is perfectly reflecting and may contain a triangularly-shaped ridge. The quantity r_C denotes the horizontal distance from the source to the center of the ridge, z_C denotes the maximum ridge height which occurs at range r_C, and z_r corresponds to the height of any point on the ridge surface above the ground plane ($z = 0$ m). The ridge slope closest to the source will be called the near side, while the opposite slope will be called the far side. The point at which the slopes intersect the ground plane will be called the near-

or far-side bases, while the point at which the two slopes intersect will be referred to as the ridge crest. In this paper we assume that the sound speed is independent of azimuth, and we require that the source $\mathcal{S}$ and receiver $\mathcal{R}$ lie in the vertical plane perpendicular to the ridge as well as the wind velocity so that we need consider only with two-dimensional sound propagation. The time-independent wave field, denoted as $A(r,z)$, is obtained by assuming that the source is harmonic with frequency f, so that $p = A\exp(2\pi i f t)$, where t is time. In the source-receiver plane, it can be shown[15] that A satisfies the reduced wave equation

$$\nabla^2 A + k_0^2 n^2 A + 2ik_0^2 n^2 \frac{v}{c_0} A_r - 2i\frac{k_0}{c_0}\frac{dv}{dz} A_{zr} = 0, \tag{1}$$

where c_0 is a reference sound speed, $k_0 = 2\pi f/c_0$ is a reference wave number, $c(r,z)$ is sound speed, $n(r,z) = c_0/c(r,z)$ is the index of refraction, and $v(r,z)$ is the horizontal component of wind velocity. Equation (1) neglects vertical components of the wind velocity. Furthermore, it can be shown that, away from the source, the quantity A takes the asymptotic form

$$A = \psi \frac{e^{ik_0 r}}{\sqrt{k_0 r}}. \tag{2}$$

Equation (2) is an essential feature of the parabolic approximation, where the quantity ψ is related to the slow-scale (i.e. many-wavelength) variation in acoustic pressure. In addition, through careful scaling and asymptotic arguments, it can also be shown that ψ satisfies one of a family of parabolic equations (PEs). Details of the derivation of this family in an inhomogeneous moving medium can be found in Refs. 15 and 16. For the numerical examples considered in the next section, the appropriate member of this family is given by

$$2ik_0\psi_r + \psi_{zz} + k_0^2(\tilde{n}^2 - 1)\psi = 0, \tag{3}$$

where

$$\tilde{n} = c_0/\tilde{c}, \tag{4}$$

with

$$\tilde{c} = c + v(r,z). \tag{5}$$

The quantity $\tilde{c}$ is called the *effective sound speed profile* (ESSP).[15]

It can be argued that the wind speed over a horizontal plane has the logarithmic form

$$v = a \ln(1 + z/z_0), \tag{6}$$

where z_0 is a scale thickness typically chosen to be 0.1 m over relatively smooth ground surfaces. The parameter a is selected so that v assumes a free-stream speed v_0 at a specified height h above the ground. Thus,

$$a = v_0[\ln(1 + h/z_0)]^{-1}. \tag{7}$$

When propagating over an irregular terrain such as the ridge shown in Fig. 1, Eq. (6) should be modified in some way to account for a range-dependent variation in the flow. If the ridge slope is not too steep, then it is reasonable to suppose that the logarithmic shape of the horizontal profile is preserved. Therefore, we modify Eq. (6) in the following way. We require that the volume flow per unit time through a cross-section of the atmosphere remain constant, and that the no-slip condition of Eq. (6) at $z = 0$ be preserved at every point along the ridge. Because of the homogeneity of the atmosphere, we can use Eq. (6) to conclude that the volume flow away from the ridge is

$$\int_0^h a \ln(1 + z/z_0) dz = \mathcal{K}, \tag{8}$$

where our waveguide extend is taken to extend to height h, as shown in Fig. 1. To conserve volume flow above the ridge, we therefore require that

$$\int_{z_r}^h b(r) \ln[1 + (z - z_r)/z_0] dz = \mathcal{K}, \tag{9}$$

where $b(r)$ is a function to be determined and z_r is the elevation of a point on the ridge. Solving Eq. (9) for $b(r)$ we obtain

$$b(r) = \mathcal{K} \{z_0 + z_0 (-[1 + (h - z_r)/z_0] + \ln[1 + (h - z_r)/z_0][1 + (h - z_r)/z_0])\}^{-1}, \tag{10}$$

and our modified velocity profile anywhere above the ridge is thus given by

$$v = b(r) \ln[1 + (z - z_r)/z_0]. \tag{11}$$

One numerical consequence of Eq. (11) is that, if the maximum speed velocity is 14.0 m s^{-1} over horizontal ground, then the highest free stream velocity is approximately 16 m s^{-1} above the ridge.

2. SIMULATION RESULTS

Our implementation of Eq. (3) is called NIFD (NASA Implicit Finite Difference). It is based upon the implicit finite difference model described in Ref. 17, together with enhancements described by us elsewhere.[6] The Crank-Nicholson scheme used to march the solution forward in range is well-suited to many propagation situations to include those with irregularly-shaped boundaries or locally-reacting surfaces. From this algorithm, we first determine ψ. Then A from Eq. (2) is the complex-valued pressure field, from which the relative intensity $I(r, z)$ is given by

$$I = 20 \log_{10} \left| \frac{A(r, z)}{A_{\text{ref}}} \right|, \tag{12}$$

where A_{ref} is a reference level at 1 m from the source.

Figure 1 depicts an idealized atmospheric acoustic waveguide. We note here that this waveguide is similar to one used as a model in Ref. 1, a study of the downwind propagation of low frequency noise from a wind turbine located at a test site in Wyoming. A cw sound source is located $h_S = 40$ m above a horizontal, perfectly-reflecting ground surface. In many of our examples, the receiver will be located on the ground surface ($z_r = 0$) and the air is assumed to be isospeed with $c_0 = 330$ m s^{-1}. The atmosphere will be taken in Subsection B to move with a logarithmic velocity profile described in Sec. I. As shown in the figure, the channel is bounded above by a horizontal, artificial, pressure-release surface of height $h = 1000$ m, beneath which is an artificial absorbing layer of thickness 500 m. This absorbing layer is designed to eliminate reflections that would otherwise occur from the pressure-release surface at the top of the waveguide. This technique is used to simulate bottom boundary conditions in ocean acoustics,[17] and, modified by us as described here, is a feature of NIFD, the numerical implementation which we use for our calculations. In all examples, a gaussian starting field is utilized to provide the initial range condition for the model.

A. Quiescent Atmosphere

We now proceed to examine a variety of effects caused by the presence of a triangular ridge type as described in Sec. I. We begin by comparing results for a ridge present and absent when the atmospheres are identical and when the source frequency is fixed at $f = 10$ Hz. Figure 2 displays relative intensity I versus range r for a source height of $h_S = 40$ m, a receiver on the ground ($h_R = 0$ m), and for a quiescent atmosphere. The source-ridge distance is $r_C = 4$ km. The ridge ascends with an inclination angle of 11.3 deg to a height of $z_C = 100$ m and spans a horizontal distance of 1 km. This particular choice of ridge slope ensures that the ridge bases coincide with the discrete mesh points used by the finite-difference implementation employed for generating numerical solutions of our PE. The solid curve denotes the intensity calculated at the earth-air interface with the ridge present, while the dotted curve corresponds to the same quantity computed without a ridge. Note first that the two curves are exactly coincident for $r \leq 3.5$ km because the parabolic approximation does not include any backscattering. On the near side of the ridge, intensity rises very sharply and then almost levels off as the receiver moves to the ridge crest. The intensity increase relative to the dotted reference curve is about +5 dB. On the far side, intensity decreases rapidly because the ridge casts an acoustic shadow. The lowest intensity level occurs at $r = 4.5$ km corresponding to the base of the far side. The total intensity change resulting from the presence of the ridge crest is about 10 dB. As the receiver moves further away from the far-side base, intensity rises sharply again, and then begins to decrease at the geometric spreading rate. Beyond about 5 km, the solid curve is approximately 1 dB below the reference curve, suggesting that the effective shadow of this particular ridge is rather weak. In other words, the signal in some sense pays only a 1 dB shadow "penalty". Naturally, the shadowing effect will be stronger at higher frequencies. In Fig. 3, the source frequency has been raised one octave to 20 Hz. On the near side of the ridge, there is still an intensity increase, but we observe that it occurs *before* the crest. Intensity then decreases as the source moves over the crest and into the shadow zone. At the far-side base, intensity

has decreased almost 20 dB below its peak value, roughly double that in the previous case. Then, as the receiver moves away from the far-side base, intensity increases and geometric spreading-loss behavior again appears. In this case, the difference between the solid curve and the reference level is about 5 dB, substantially stronger than the shadow experienced in the 10 Hz case.

Despite the results in Fig. 2, shadowing behind ridges can be significant at 10 Hz, as demonstrated in Fig. 4. Here, intensity calculations are shown for three source-ridge distances: r_C = 1, 4, and 7 km. In each instance, the ridge dimensions have been kept fixed. Note that, for source-ridge distances of 4 and 7 km, the shadowing on the far sides is virtually identical. However, for the closest ridge, the far-side shadowing is much stronger. Furthermore, we note that the intensity rise on the near side slope of the 1 km ridge is more similar to the solid curve in Fig. 3 in that the peak intensity value occurs before the ridge peak is reached.

Intensity also possesses a substantial amount of vertical structure as shown in Fig. 5, which illustrates the variation of intensity with receiver height h_R for five fixed range levels. At the near-side base (r = 3.5 km) I decreases very slowly with increasing h_R. At the ridge crest (r = 4 km), there is a very rapid intensity variation of over 15 dB. Behind the ridge, we see that the intensity vs. height curves exhibit distinctive interference patterns, suggesting that the acoustic field behind the ridge is fairly complicated. For example, at r = 6 km, intensity decreases by about 8 dB as h_R increases to 150 m and then begins to increase again. As noted in the discussion of Fig. 2, the residual shadowing caused by the ridge at that range is small when the receiver is placed on the ground. Yet at that same range, ridge effects can be substantially stronger at larger receiver heights. These results suggest that for very low frequency sources, especially for frequencies as low as 10 Hz, in quiescent, isospeed atmospheres, large ridgelines have their strongest effects if the source-ridge distance z_C is small. Beyond r = 4 km, the far side shadowing is rather weak. This could have practical ramifications. For example, to minimize signal strength of low-frequency sources, an important source of environmental noise,[4] it may not be sufficient to locate the

source so that a hill or ridge is between the source and, say, a residential community. In some cases, these kinds of topographical features may have little or no effect.

B. Receiver Downwind

Figure 6 permits a comparison between propagation with and without a ridge in the presence of a wind. The receiver is downwind from the source and the freestream windspeed $v_0 = 6$ m s^{-1}. The dotted curve corresponds to the intensity calculated without the ridge present. We note that this curve corresponds to a substantially higher level than the analogous one in Fig. 2, since the wind profile serves to trap sound energy in a strongly-focusing ground waveguide. When the ridge is present, I increases on the near-side slope and reaches its largest value before the crest. Intensity falls off sharply and then rises again once the ground plane is reached. However, the intensity rise does not return to the reference level as occured in the no-wind case depicted in Fig. 2. Rather, there is a strong acoustic shadow behind the ridge and, surprisingly, the intensity decreases substantially faster behind the ridge with increasing range than it would without the ridge present even though the wind direction and structure favors the formation of a strong ground surface duct. Evidently, for this particular combination of source and topographical parameters, the diffracted field and refracted field appear to engage in some sort of destructive interference.

The far side sound field pattern is sensitive to wind speed as demonstrated in Fig. 7. Three different wind profiles are used to construct the intensity curves shown in the figure. As free-stream wind speed increases, intensity levels are elevated on the near side, as expected. The shadowing tends to be stronger on the far side as wind speed increases, but, for free-stream speeds of 10 and 14 m s^{-1}, a clear interference pattern emerges behind the ridge, supporting the observation made above that there seems to be evidence of interference between the diffracted and refracted sound fields behind the ridge. Additional insight into this phenomenon can be seen in Fig. 8. In this example, the free-stream wind speed is held fixed at 10 m s^{-1}, but the intensity is computed for three source frequencies. On the near side of the ridge, interference patterns emerge as the frequency is increased, and intensity

fluctuations are substantially more complex on the near side slope. Beyond the far side, the spatial periodicity of each curve appears to double with frequency. As before, this is consistent with the possible interference between the diffracted and refracted acoustic fields. These results could have interesting and important consequences. For example, even though ridges may afford little protection from low frequency noise sources, if a prevailing wind is present, the ridge effectively negates the heightened intensity levels that might otherwise occur. This result may be useful in the selection of sites for large wind turbines.

The vertical structure of the sound field, when the wind blows from source to receiver, is depicted in Fig. 9 for five different receiver ranges. At the near-side base, intensity decreases sharply with increasing h_R, a characteristic of a ground waveguide. The thin solid curve, denoting intensity at the ridge crest, reveals a more complicated structure. At the base of the far side, where $r = 4.5$ km, the decrease in I with increasing h_R weakens noticeably. It strengthens at $r = 5$ km and weakens somewhat beyond that range. For potential target-detection applications in the presence of a wind and a source-receiver wind, extensions of these results might suggest that the best place to position the receiver, regardless of range, is on the ground surface.

C. Receiver Upwind

The sound field also possesses unexpected features behind a ridge when the receiver is upwind from the source (i.e. the wind is directed toward the source). In Fig. 10, I is displayed for a 6 m s^{-1} free-stream wind with and without a ridge. The latter case, shown as the dotted curve, again serves as a reference level. A comparison of the relative levels in Figs. 2 and 6 shows that relative intensity decreases much more rapidly with increasing range in the upwind case because the wind profile acts to refract sound away from the ground. For sufficiently high frequencies, a virtual shadow zone can be shown to be formed at relatively short distances from the source. Even at 10 Hz, however, the upwind sound field is strongly attenuated by the wind profile. The intensity increases on the near-side slope, decreases on the far side, but then rises again to a level significantly *higher* than the reference level. At

relatively close distances behind the ridge, the diffracted sound field is at least 5 dB larger than the reference sound field. This is exactly the opposite effect observed in the downwind case.

The strength of this "negative" shadow in the upwind case also depends on wind speed, as shown in Fig. 11. The far-side intensity levels are clearly elevated at both 6 and 10 m s^{-1} free-stream wind speeds. For $v_0 = 14$ m s^{-1} the intensity structure seems to be somewhat erratic behind the ridge. Because intensity levels are so small (in the absolute sense), it would seem that this structure may be partially attribuatable to the emergence of numerical roundoff errors. The vertical structure of the upwind sound field near the ridge is shown in Fig. 12. At the near-side base, where $r = 3.5$ km, I increases as h_R increases and this characteristic behavior is more or less observed at the other ranges shown in the figure. The sound field appears to possesses less structure that in both the no-wind and downwind examples discussed previously (see Figs. 5 and 9). It is useful to note that, in the upwind situation, signal strength can generally be increased by raising the receiver off the ground. For target acquisition applications, this indicates that further calculations may suggest that an airborne receiver, such as one suspended from a balloon, could enhance the likelihood of sensing the presence of a sound source in the presence of a ridge and an upwind flow.

SUMMARY

We examine the effects of a triangularly-shaped ridge on low-frequency cw acoustic propagation in both a quiescent and windy atmosphere, using the parabolic approximation. A logarithmic wind-speed profile is modified and used to model an atmospheric flow over the ridge. This profile is employed to determine the effective sound-speed profile which is used as the primary environmental input to an implicit finite-difference implemenation of the parabolic approximation. In a quiescent atmosphere, numerical simulations suggest that the acoustic shadow behind a ridge is fairly weak at low frequencies, unless the source-ridge distance is small. When the receiver is behind the ridge and also downwind from the source, the ridge can cast a very deep sound shadow. That is, the relative intensity of the acoustic field

behind the ridge is substantially lower than it would be if the ridge were not present. In addition, the sound-field structure is altered considerably, particularly as the source frequency is raised. When the wind direction is reversed, our results indicate that the intensity behind the ridge is substantially higher than it would be without the ridge. Further, diffraction of the acoustic field behind a ridge, in the presence of a refracting wind profile, can alter the nature of the field in unexpected ways.

REFERENCES

[1] Hawkins, J.A., Application of ray theory to propagation of low frequency noise from wind turbines. NASA Langley Res. Center, Hampton, VA, CR-178367, 1987.

[2] Dommermuth, F. & Schiller, J., Estimating the trajectory of an accelerationless aircraft by means of a stationary acoustic sensor. *J. Acoust. Soc. Am.* **76** (1984) 1114–1122.

[3] Dommermuth, F., The estimation of target motion parameters from cpa time measurements in a field of acoustic sensors. *J. Acoust. Soc. Am.* **83** (1988) 1476–1480.

[4] Schomer, P.D. & Averbuch, A., Indoor human response to blast sounds that generate rattles. *J. Acoust. Soc. Am.* **86** (1989) 665–673.

[5] Robertson, J.S., Jacobson, M.J., & Siegmann, W.L., Mathematical modeling of sound propagation in the atmosphere using the parabolic approximation, in *Transactions of the Sixth Army Conference on Applied Mathematics & Computing*, ARO Report 89–1, U.S. Army Research Office, Research Triangle Park, NC, 1989.

[6] Robertson, J.S., Jacobson, M.J., & Siegmann, W.L., Low-frequency sound propagation modeling over a locally-reacting boundary using the parabolic approximation. Submitted to *J. Acoust. Soc. Am.*

[7] Gilbert, K. & White, M., Application of the parabolic equation to sound propagation in a refracting atmosphere. *J. Acoust. Soc. Am.* **85** (1989) 630–637.

[8] White, M.J. & Gilbert, K.E., Application of the parabolic equation to the outdoor propagation of sound. *Appl. Acoust.* **27** (1989) 227–238.

[9] Malbéqui P. & Jouaillec, F., Acoustic propagation over the ground using the parabolic approximation, to appear in *Proceedings, INTERNOISE 88.*

[10] Tolstoy, I., Exact, explicit solutions for diffraction by hard sound barriers & seamounts, *J. Acoust. Soc. Am.* **85** (1989) 661–669.

[11] Tappert, F.D., The parabolic approximation method, in *Wave Propagation & Underwater Acoustics*, edited by Keller, J.B. and Papadakis, J.S., Springer, Berlin, 1977, pp. 224–287.

[12] Ebbeson, G.R. & Turner, R.G., Sound propagation over Dickins Seamount in the Northeast Pacific Ocean. *J. Acoust. Soc. Am.* **73** (1983) 143–152.

[13] Rasmussen, K.B., On the effect of terrain profiles on sound propagation outdoors. *J. Sound Vib.* **98** (1985) 35–44.

[14] DeJong, B.A., Moerkerken, A., & van der Toorn, J.D., Propagation of sound over grassland & over an earth barrier, *J. Sound Vib.* **86** (1983) 23–46.

[15] Robertson, J.S., Siegmann, W.L., & Jacobson, M.J., Current & current shear effects in the parabolic approximation for underwater sound channels. *J. Acoust. Soc. Am.* **77** (1985) 1768–1780.

[16] Robertson, J.S., Siegmann, W.L., & Jacobson, M.J., Acoustical effects of ocean current shear structures in the parabolic approximation. *J. Acoust. Soc. Am.* **82** (1987) 559–573.

[17] Lee, D. & McDaniel, S.T., Ocean acoustic propagation by finite difference methods. *Comp. & Maths. with Appls.* **14** (1987) 305–423.

FIGURE LEGENDS

FIG. 1. Atmospheric sound channel.

FIG. 2. Relative intensity I vs. range r; no wind; $f = 10$ Hz, $r_C = 4$ km, $z_C = 100$ m, $h_S = 40$ m, $h_R = 0$ m.

FIG. 3. Relative intensity I vs. range r; no wind; $f = 20$ Hz; other parameters as in Fig. 2.

FIG. 4. Relative intensity I vs. range r for three values of r_C; no wind; $f = 10$ Hz; other parameters as in Fig. 2.

FIG. 5. Relative intensity I vs. receiver height h_R for five source-receiver ranges r; no wind; other parameters as in Fig. 2.

FIG. 6. Relative intensity I vs. range r; receiver downwind and $v_0 = 10$ m s^{-1}; other parameters as in Fig. 2.

FIG. 7. Relative intensity I vs. range r for receiver downwind and three values of v_0; other parameters as in Fig. 2.

FIG. 8. Relative intensity I vs. range r for three values of frequency f; receiver downwind, $v_0 = 10$ m s^{-1}; other parameters as in Fig. 2.

FIG. 9. Relative intensity I vs, receiver height h_R for five source-receiver ranges r; receiver downwind; other parameters as in Fig. 2.

FIG. 10. Relative intensity I vs. range r; receiver upwind and $v_0 = 10$ m s^{-1}; other parameters as in Fig. 2.

FIG. 11. Relative intensity I vs. range r for receiver upwind and three values of v_0; other parameters as in Fig. 2.

FIG. 12. Relative intensity I vs, receiver height h_R for five source-receiver ranges r; receiver upwind; other parameters as in Fig. 2.

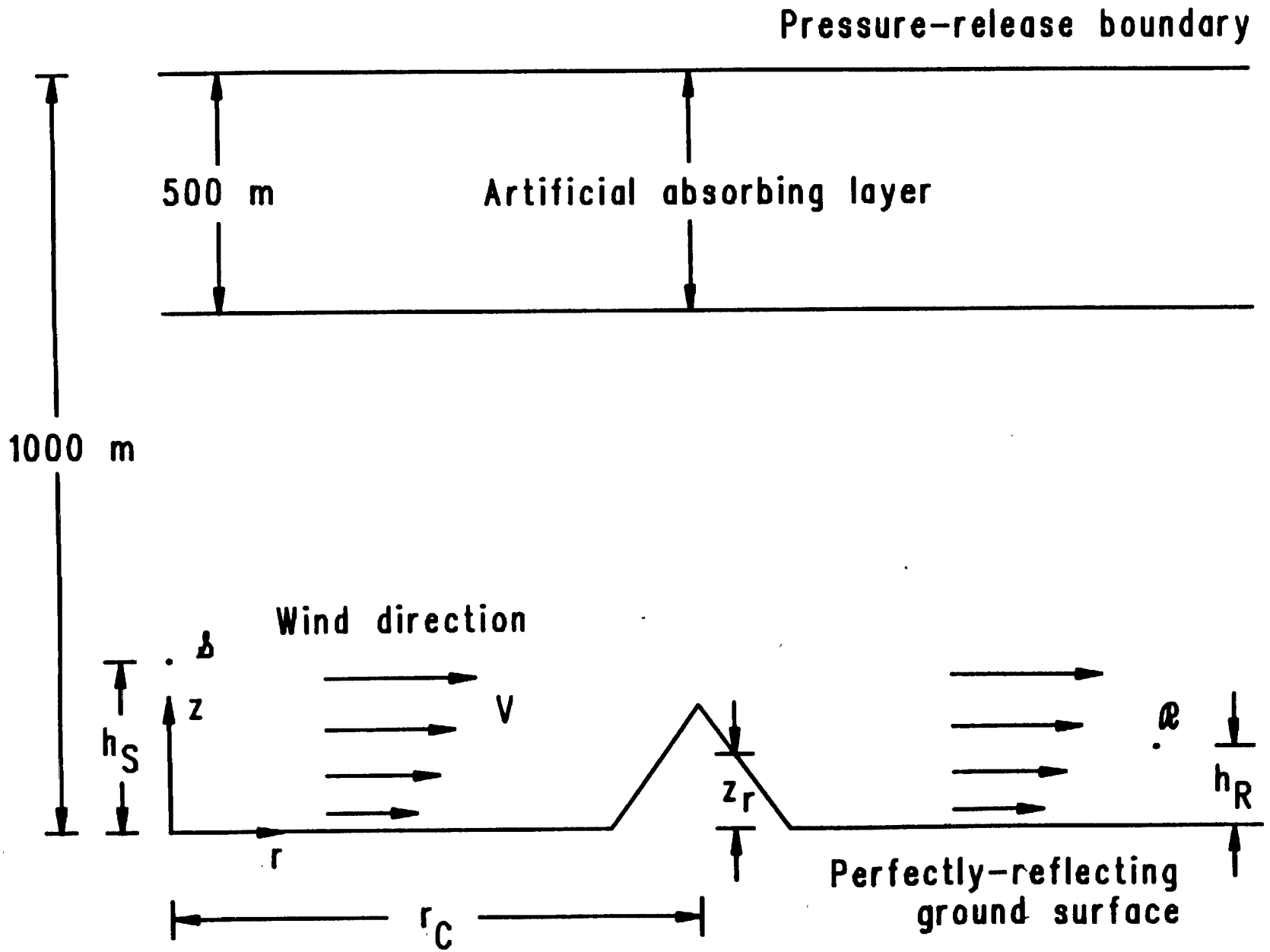
Pressure-release boundary
500 m
Artificial absorbing layer
1000 m
Wind direction
b
z
V
h_S
z_r
a
h_R
r
r_C
Perfectly-reflecting
ground surface

FIG. 1

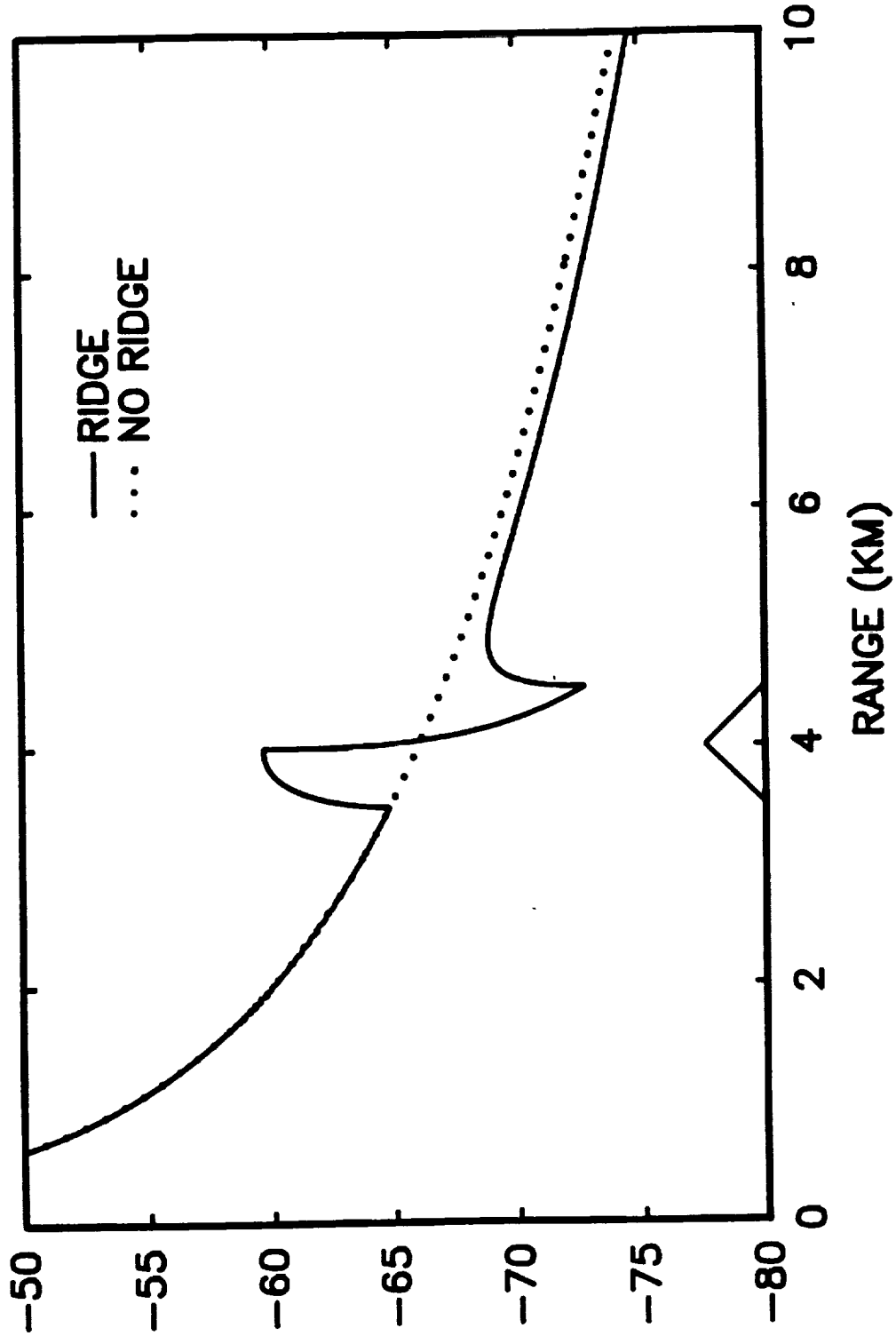
RIDGE
NO RIDGE
REL. INTENSITY (dB)
-50
-55
-60
-65
-70
-75
-80
0
2
4
6
8
10
RANGE (KM)

FIG. 2

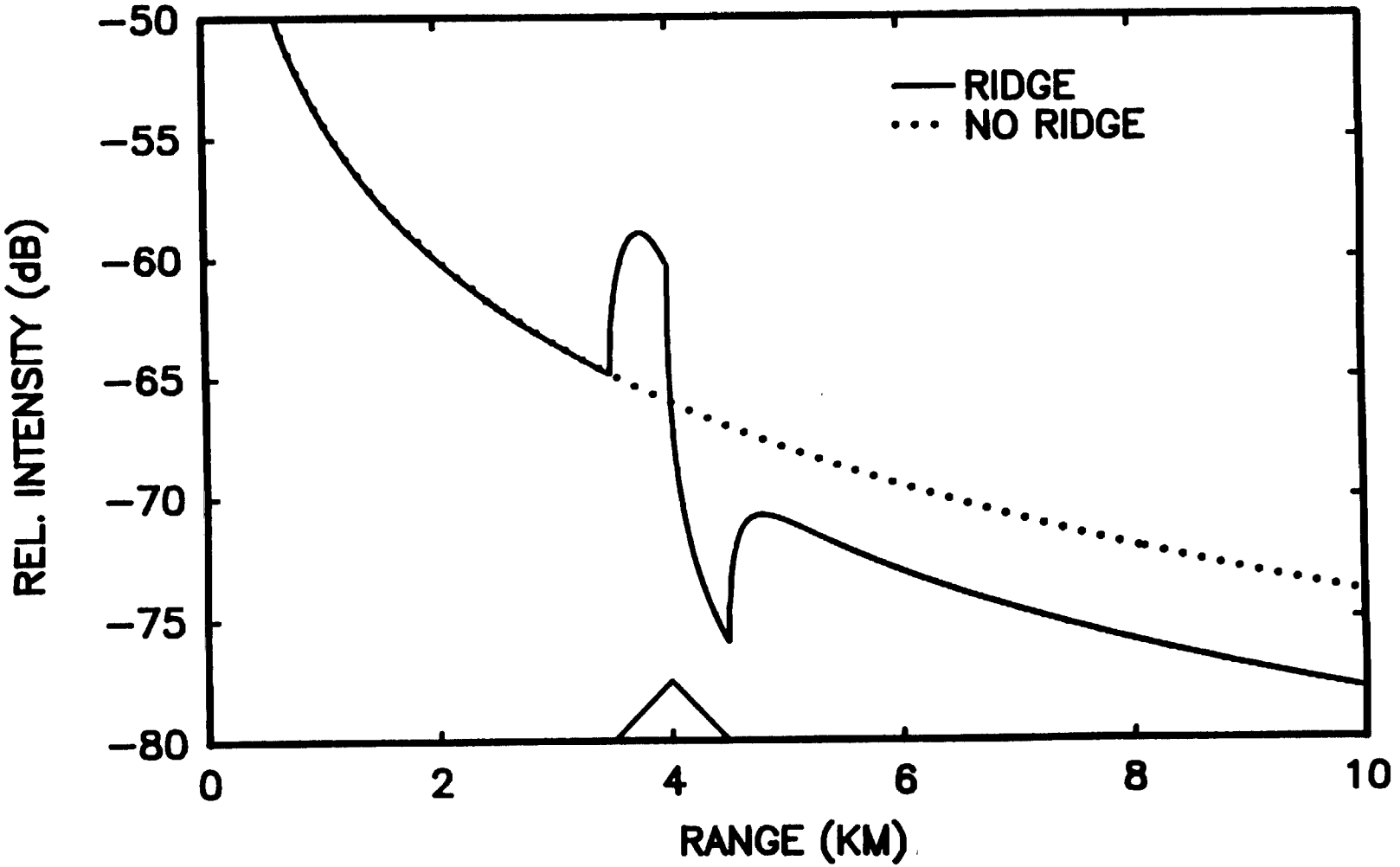
RIDGE
NO RIDGE
REL. INTENSITY (dB)
−50
−55
−60
−65
−70
−75
−80
0
2
4
6
8
10
RANGE (KM)

FIG. 3

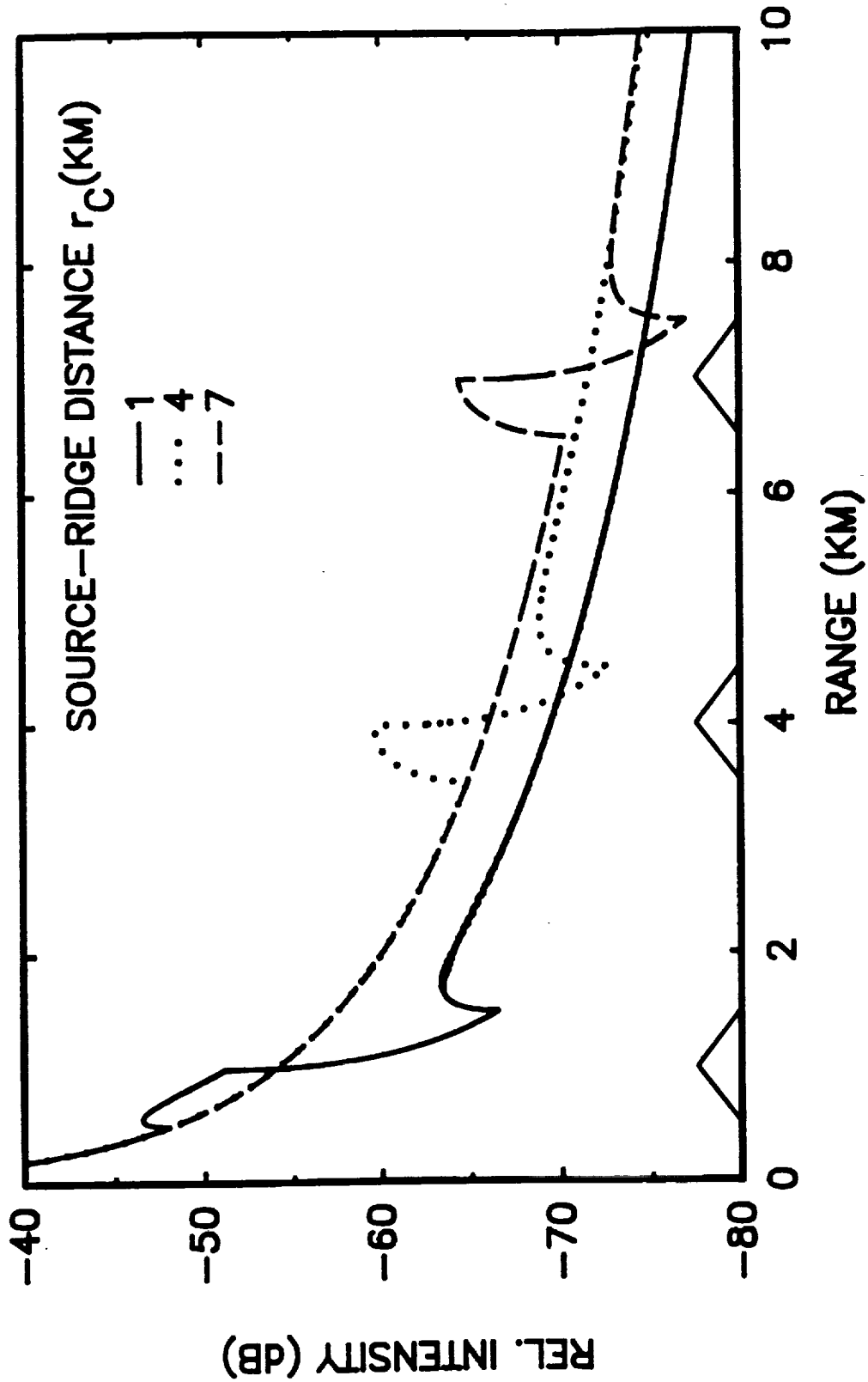
SOURCE–RIDGE DISTANCE r_C(KM)
1
4
7
REL. INTENSITY (dB)
−40
−50
−60
−70
−80
0
2
4
6
8
10
RANGE (KM)

FIG. 4

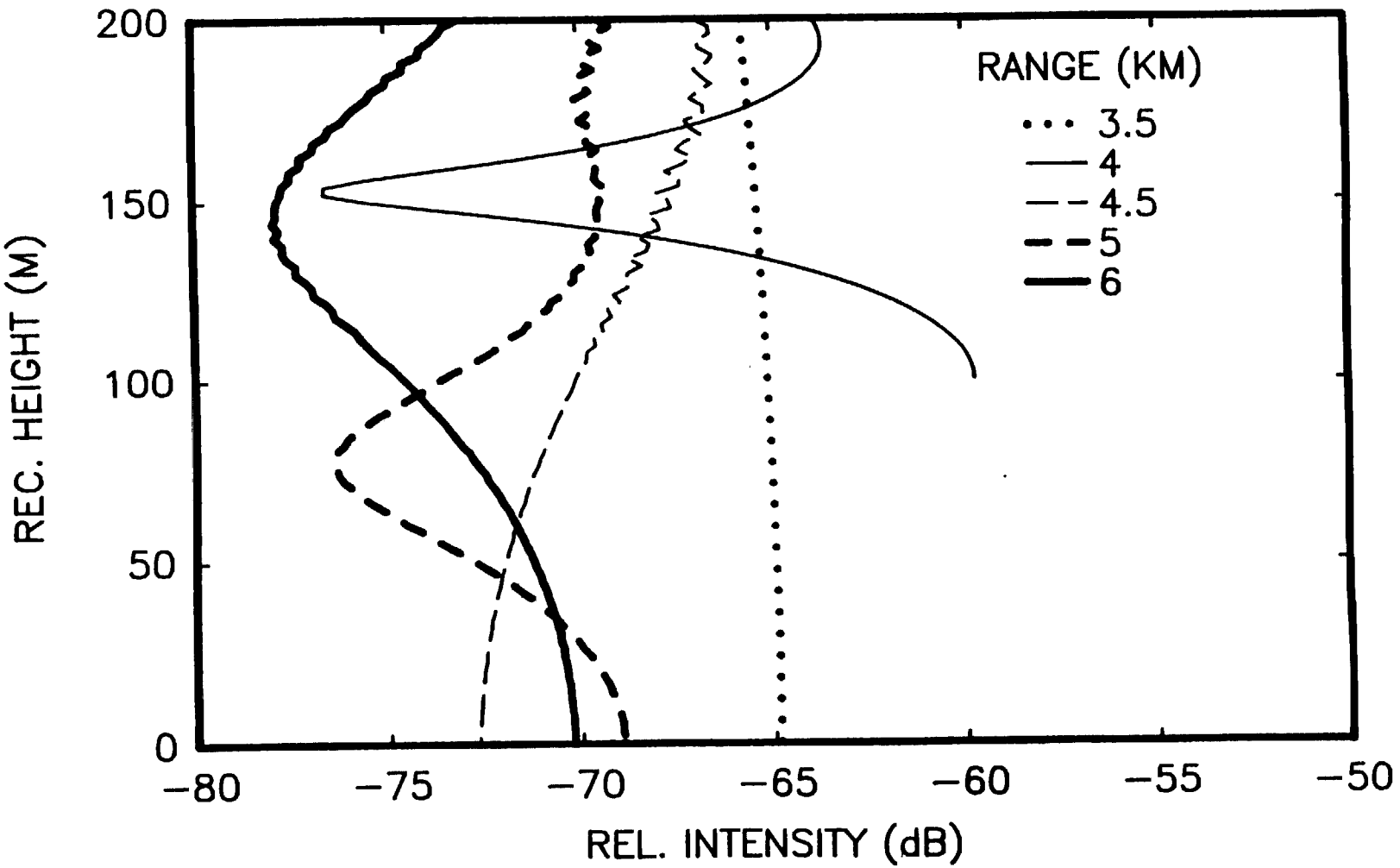
200
150
100
50
0
REC. HEIGHT (M)
−80
−75
−70
−65
−60
−55
−50
REL. INTENSITY (dB)
RANGE (KM)
3.5
4
4.5
5
6

FIG. 5

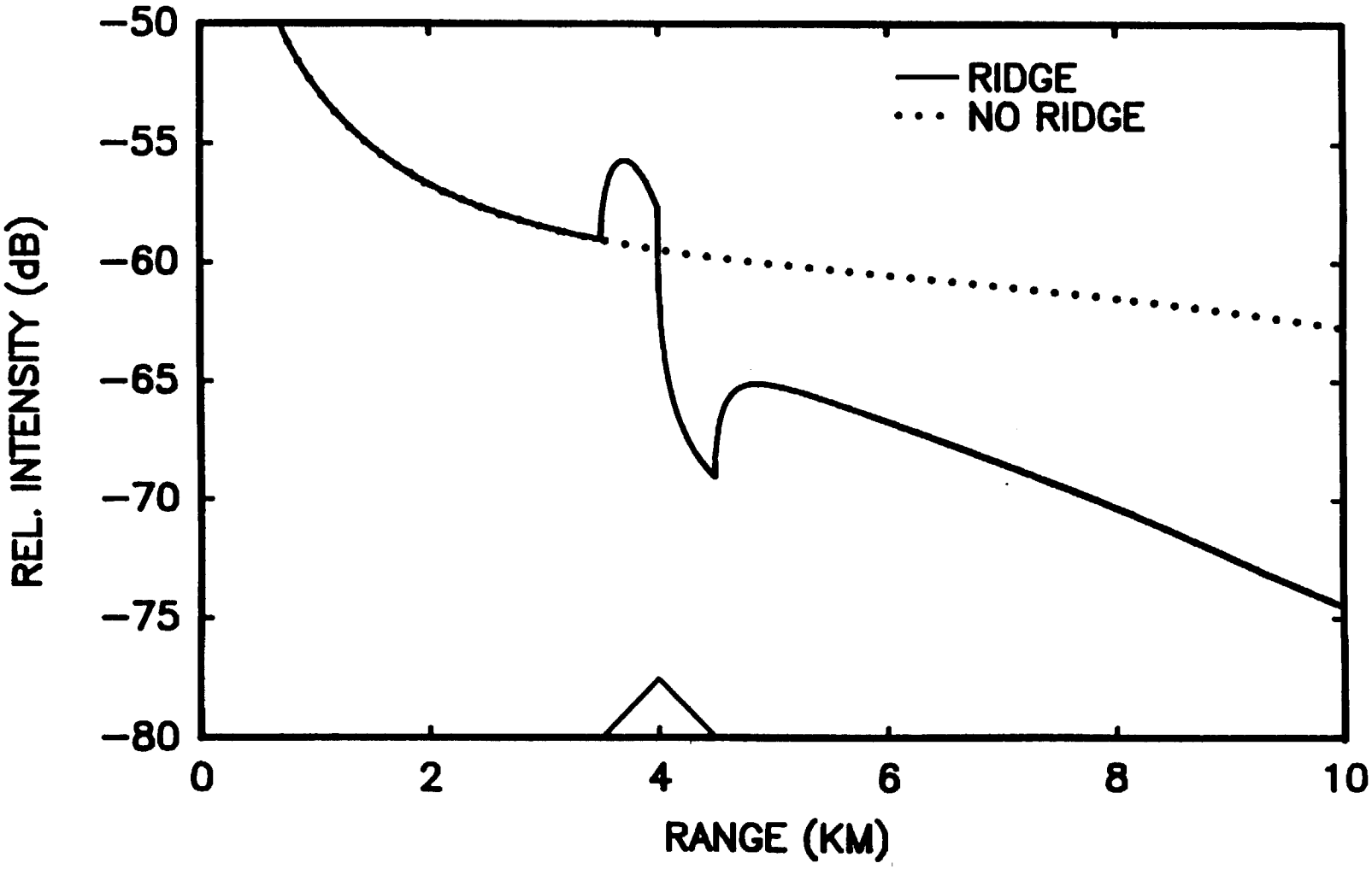
RIDGE
NO RIDGE
REL. INTENSITY (dB)
−50
−55
−60
−65
−70
−75
−80
0
2
4
6
8
10
RANGE (KM)

FIG. 6

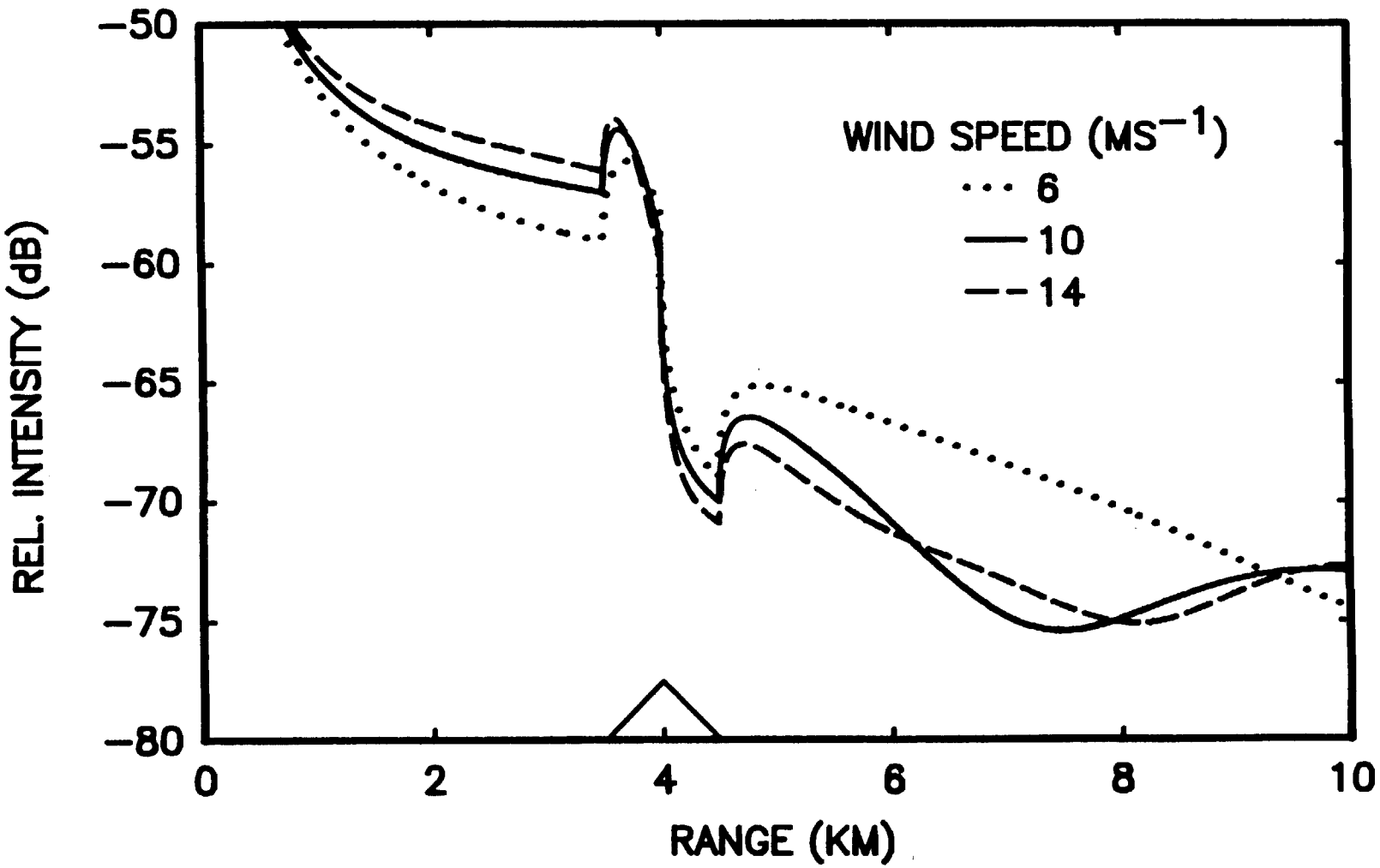
WIND SPEED (MS^{-1})
6
10
14
REL. INTENSITY (dB)
−50
−55
−60
−65
−70
−75
−80
0
2
4
6
8
10
RANGE (KM)

FIG. 7

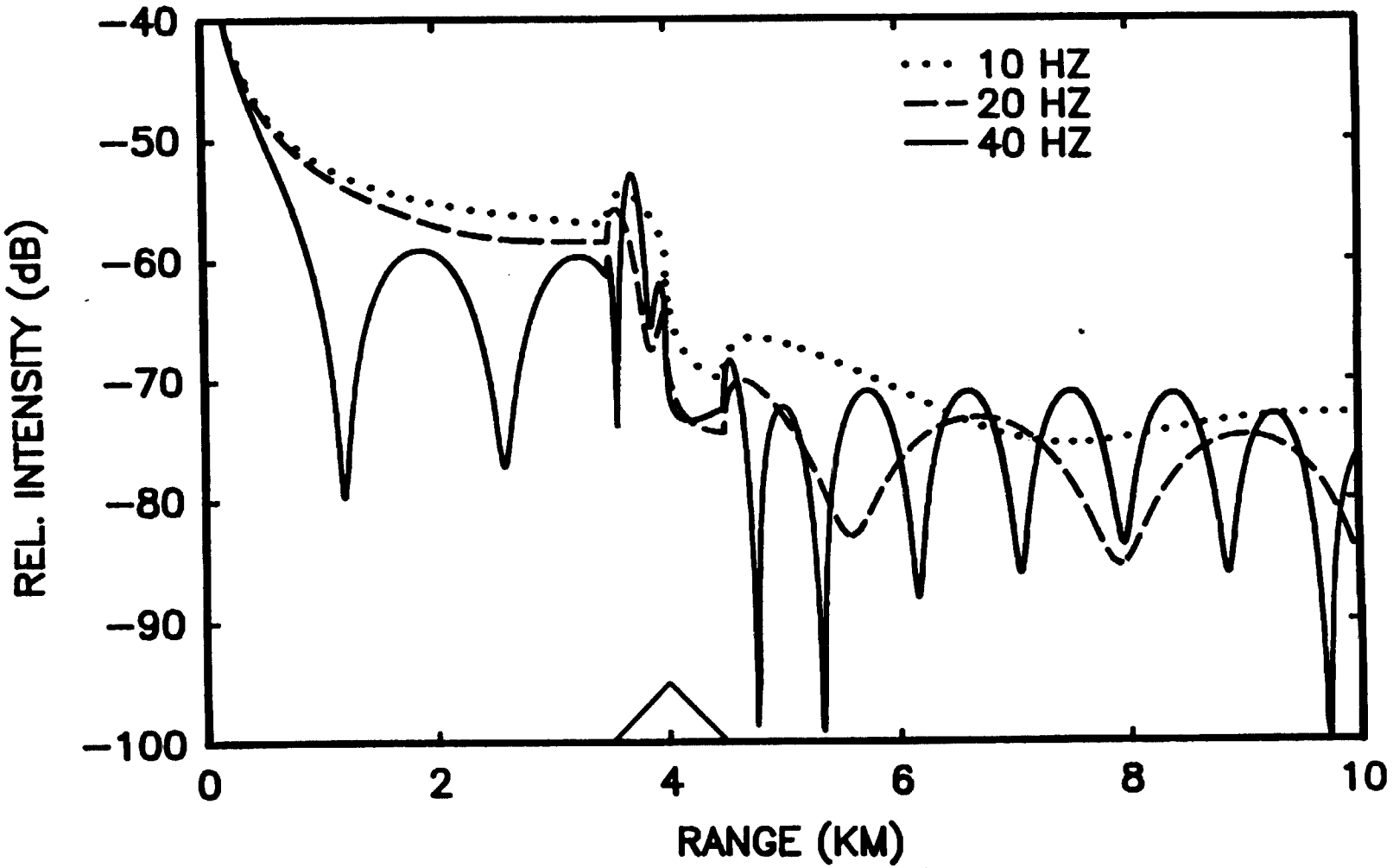
10 HZ
20 HZ
40 HZ
REL. INTENSITY (dB)
-40
-50
-60
-70
-80
-90
-100
0
2
4
6
8
10
RANGE (KM)

FIG. 8

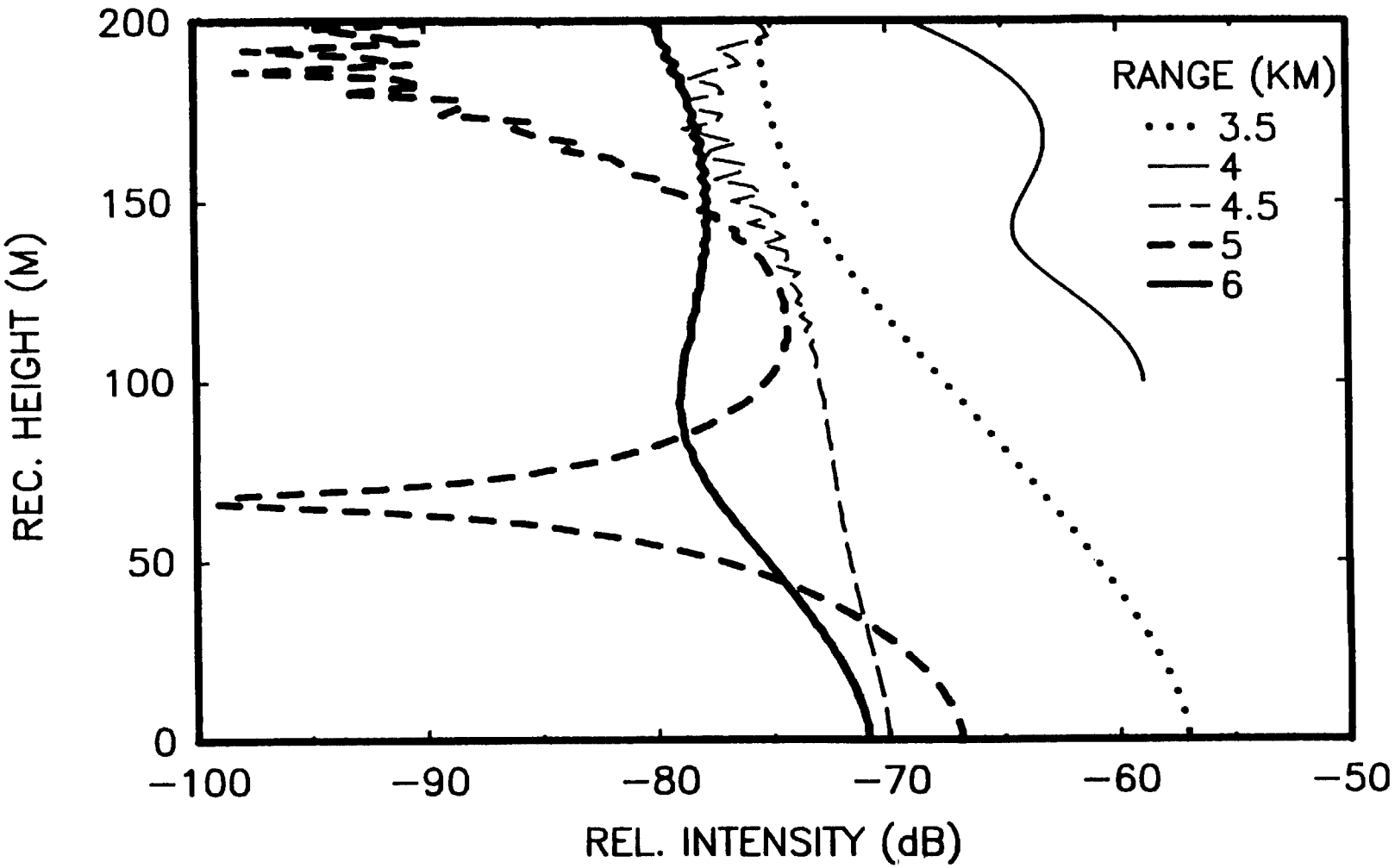
200
150
100
50
0
REC. HEIGHT (M)
−100
−90
−80
−70
−60
−50
REL. INTENSITY (dB)
RANGE (KM)
3.5
4
4.5
5
6

FIG. 9

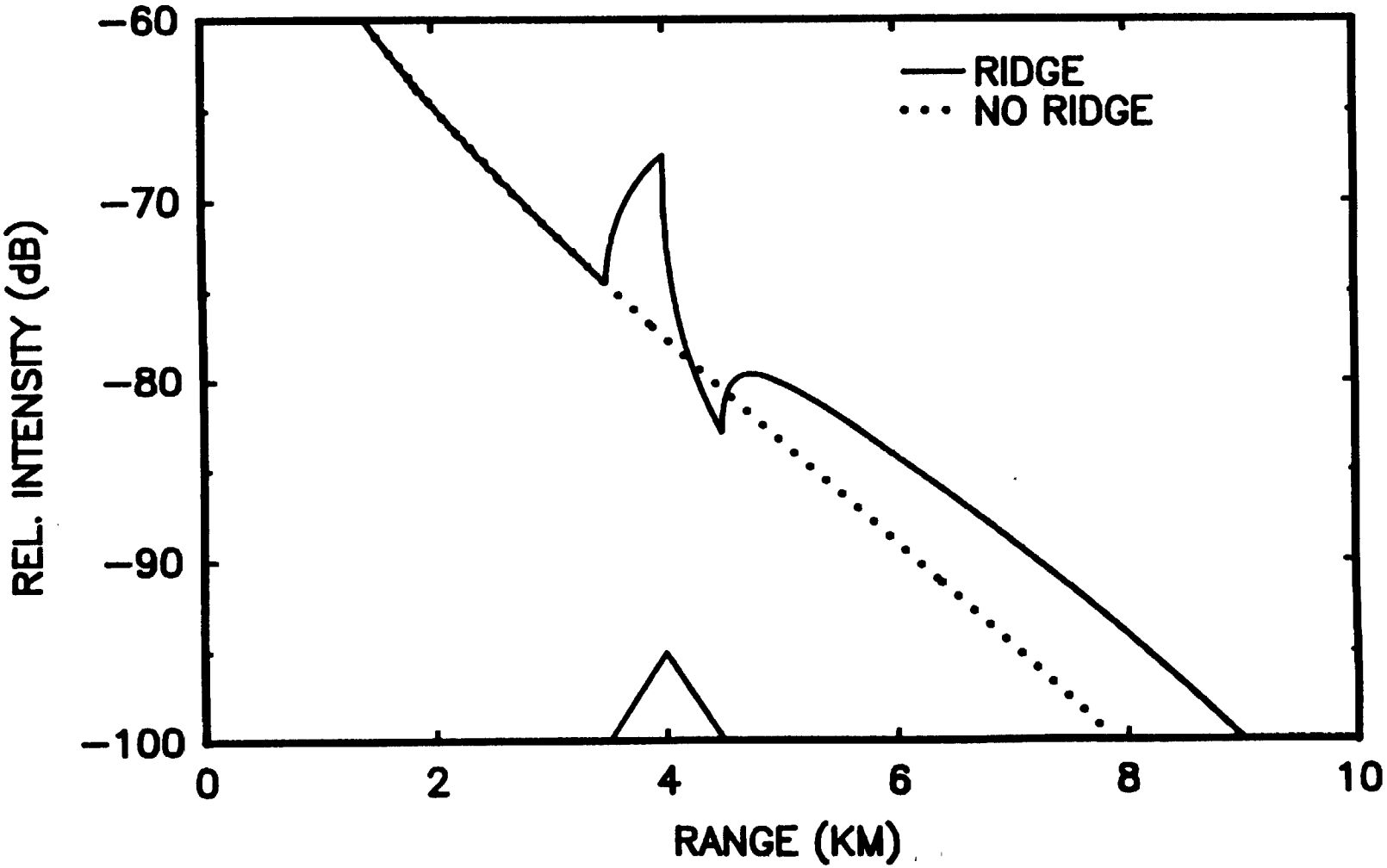
RIDGE
NO RIDGE
REL. INTENSITY (dB)
-60
-70
-80
-90
-100
0
2
4
6
8
10
RANGE (KM)

FIG. 10

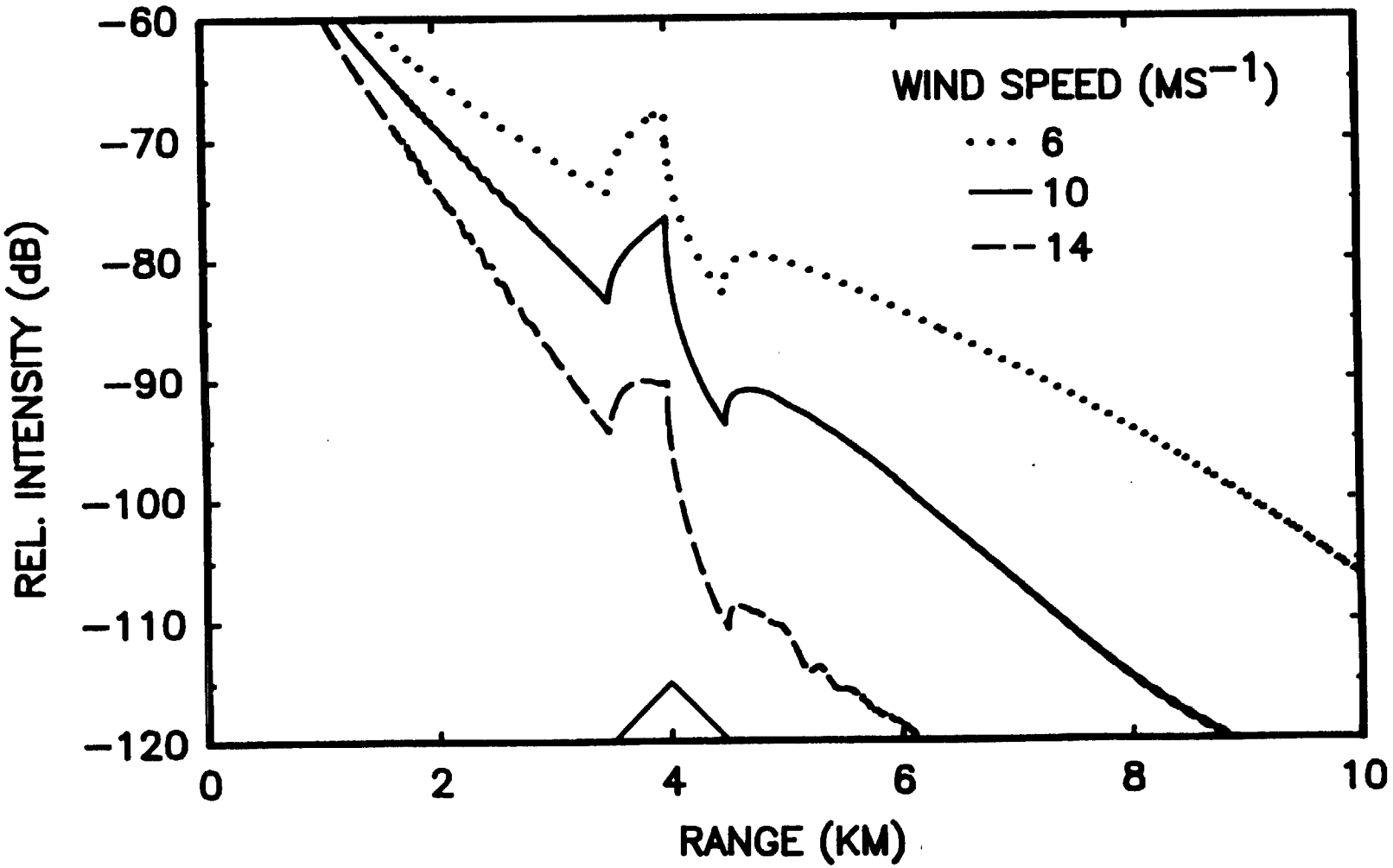
WIND SPEED (MS^{-1})
6
10
14
REL. INTENSITY (dB)
−60
−70
−80
−90
−100
−110
−120
0
2
4
6
8
10
RANGE (KM)

FIG. 11

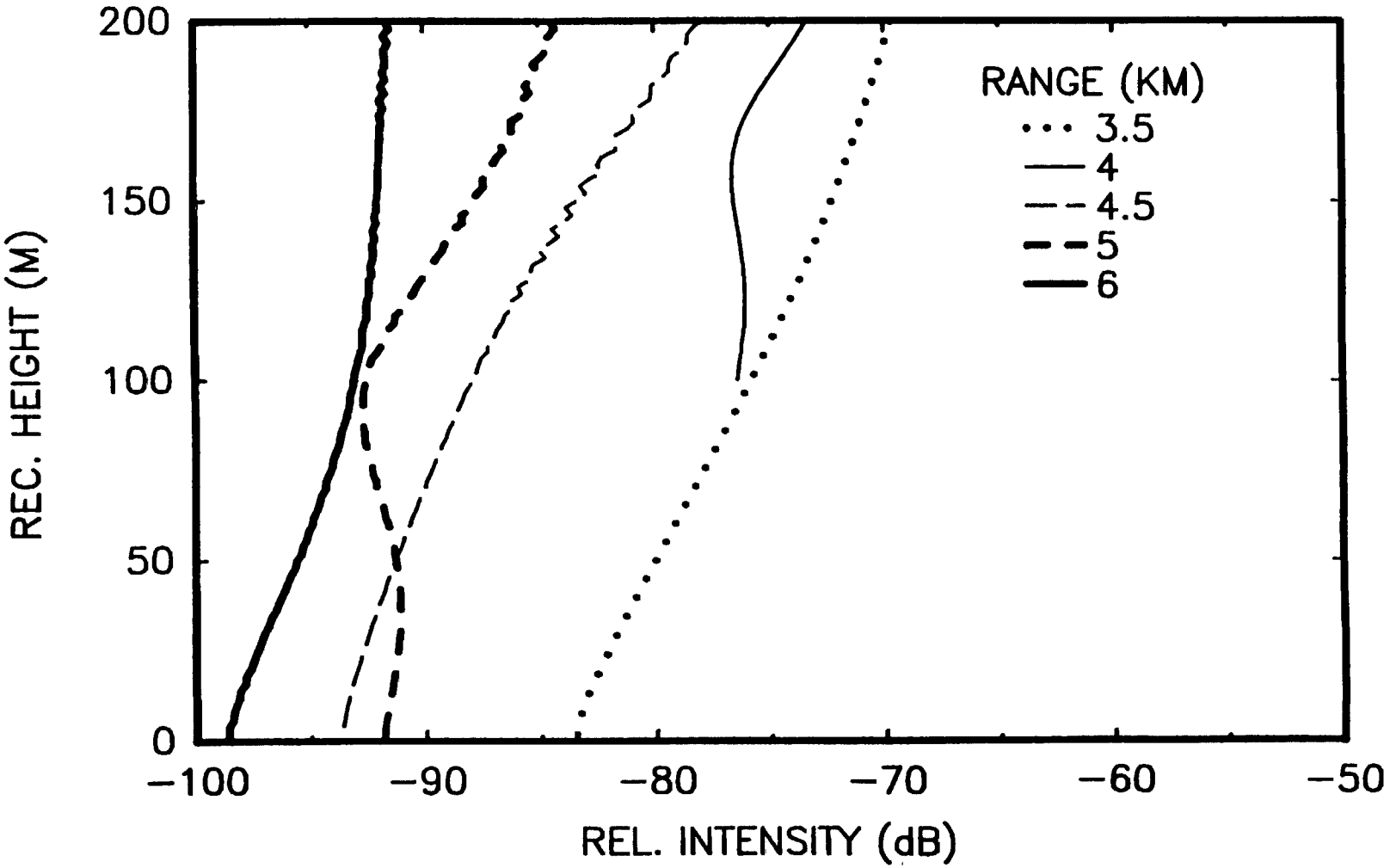
200
150
100
50
0
REC. HEIGHT (M)
−100
−90
−80
−70
−60
−50
REL. INTENSITY (dB)
RANGE (KM)
3.5
4
4.5
5
6

FIG. 12

Distribution List:

NASA Langley Research Center, Applied Acoustics Branch, MS 460, Hampton, VA 23665
ATTN: Dr. Gary McAninch 3
ATTN: Mr. Arnold Mueller 1
ATTN: Mr. David Chestnutt 1

NASA Scientific and Technical Information Facility, P.O. Box 8757, Baltimore-Washington International Airport, MD 21210 2

U.S. Army Laboratory Command, ATTN: SLCTO (Dr. Norman Berg), 2800 Powder Mill Road, Adelphi, MD, 20783-1145 1

U.S. Army Atmospheric Sciences Laboratory, ATTN: SLCAS-AR-A (Dr. Richard Shirkey), White Sands Missile Range, NM 88002-5501 1

U.S. Army Research Office, Mathematical Sciences Division (Dr. Jagdish Chandra), P.O. Box 12211, Research Triangle Park, NC 27709 1

Office of Naval Research, Code 1125OA (Dr. Marshall Orr), 800 North Quincy Street, Arlington, VA 22217-5000 1

Naval Underwater Systems Center, Code 3122 (Dr. Ding Lee), New London, CT 06320 1